CHAPTER 6

SYNTHESIS AND CHARACTERIZATION OF COMPOSITES

$BaTi_{0.85}Sn_{0.15}O_3$-CNT

6.1 Introduction

Elemental carbon in the sp^2 hybridization can form a variety [190] of structures. Beside well-known graphite structure, carbon can build closed and open cages with honeycomb atomic arrangement. The first such structure discovered was the C60 molecule by Kroto et al. [191] Although various carbon cages were studied, it was only in 1991, when Iijima [192] observed for the first time tubular carbon structures. The nanotubes consisted of up to several tens of graphitic shells so called multi-walled carbon nanotubes (MWNT) with adjacent shell separation of ~0.34 nm, diameters of ~1 nm and high length/diameter ratio. Two years later, Iijima and Ichihashi [193] and Bethune et al.[194] synthesized single-walled carbon nanotubes (SWNT).

There are two main types of carbon nanotubes [195] that can have high structural perfection. Single walled nanotubes (SWNT) consist of a single graphite sheet seamlessly wrapped into a cylindrical tube (Figure 6.1 a). Multiwalled nanotubes (MWNT) comprise an array of such nanotubes that are concentrically nested like rings of a tree trunk (Figure 6.1 b). Carbon nanotubes (CNTs) are one-dimensional carbon materials with excellent mechanical, electrical, thermal and chemical stability properties. Carbon nano tubes (CNTs) high electrical conductivity (10^6 S/cm) [196], excellent carrier mobility (10^5 $cm^2/V/s$) [197], thermal conductivity above 3000W/m-K depending on its length and diameter [198], remark able mechanical properties, low density and the unique one-dimensional structures [199].

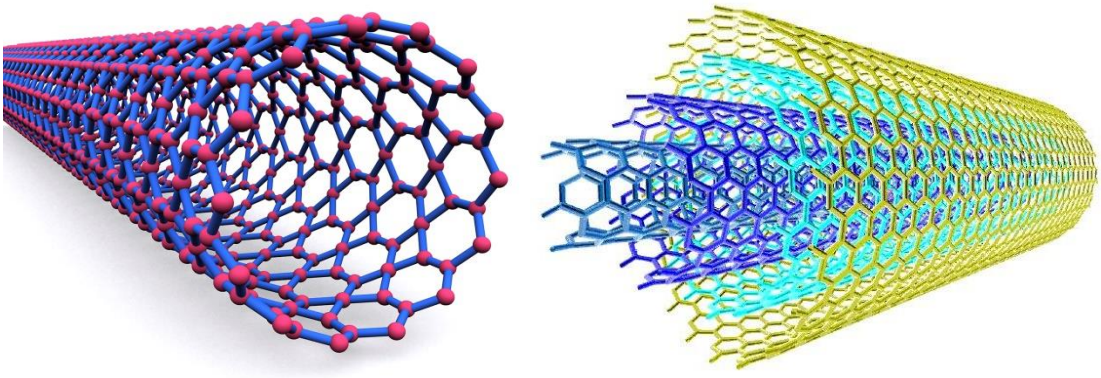

Figure 6.1 Carbon nanotube (a) single walled (b) Multiwalled Carbon nanotube

Incorporation of CNTs into ceramics/polymers/glasses has attracted interests in the last decade [200-202]. However, the study is still far from exploited due to the strong aggregation of CNTs in the matrix. Unlike carbon fibers, the as-prepared CNTs tend to form bundles due to van der Waals forces, and it is difficult to separate them individually. The effective utilization of nanotubes in composite applications depends strongly on the ability to disperse CNTs homogeneously throughout the matrix. Furthermore, good interfacial bonding is required to achieve load transfer across the CNT-matrix interface, a condition necessary for improving the mechanical properties of ceramic composites. From the viewpoint of colloidal processing, multi components could be distributed evenly when they process similar surface properties. Successful modification of CNTs by using dispersants or acid treatment proves more homogeneity in the matrix compared with that of simple mixed samples using pristine CNTs [203,204]. Hwang et al. [205] synthesized silicon glass rods by using surfactant-carbon nanotube co-micelles as templates. These glass rods were used as additives to reinforce inorganic ceramics. They showed~100% enhancement on hardness in the presence of ~6 wt% of CNTs. Gong et al. [206] reported the use of a surfactant as a processing aid to improve the dispersion of single-wall

carbon nanotubes (SWNTs) in epoxy resin, leading to a significant improvement of mechanical properties. The dispersants and acid treatment were used to modify the CNTs and then the functionalized nanotubes were incorporated into various ceramic matrices including Al_2O_3, $BaTiO_3$ and TiN. The mechanical properties of these composites have been investigated [207]. Additions of CNTs even in small amount have been beneficial for enhancing electrical conductivity, optical, mechanical and thermal properties of chalcogenide glassy alloys [208,209].

The high dielectric constant of multi-walled carbon nanotube in the (MWCNT)/$BaTiO_3$ nano-composite make it a promising candidate for improving microwave-absorbing and electromagnetic interference (EMI) shielding material with outstanding microwave attenuation characteristics [210]. Controlling nano-composite sintering behavior (porosity and densification) is critical to attaining these dielectric properties. Huang et al. [211] prepared an MWCNT/$BaTiO_3$ nano-composite ceramic by applying hot-press sintering, and reported that the high sintering temperature (1200°C) was a major technical challenge for the economical fabrication of this nano-composite. Decreasing the sintering temperature is essential to commercial production of this nano-composite. Practical techniques for decreasing the sintering temperature of ceramics densified at high temperatures include the use of materials having a finer particle size, a chemical process or doping of low-melting temperature constituents [212-213]. It appears that the latter technique, in which liquid phase-assisted contact is the predominant densification mechanism, efficiently improves sintering behavior. It also features a simple procedure that is low cost, and requires comparatively little time. As it is discussed in the previous chapters barium titanate stannate, $Ba(Ti_{1-x}Sn_x)O_3$ is a binary solid solution system composed of ferroelectric barium titanate and non-ferroelectric barium stannate. This material system may find applications, such as a capacitor, bolometer, actuator and microwave phase

shifter etc. The Curie temperature or dielectric constant of these types of system could be widely shifted by changing the wt% of tin. The permittivity is very high as well as temperature is biased field sensitive. But major problem with this system as observed by us as well other investigators that as concentration of Sn in the system increases density decreases. In order to overcome this problem and further enhance other properties such as dielectric, electric, mechanical in this work we have tried to incorporate single walled CNT in the matrix of one of the composition $BaTi_{0.85}Sn_{0.15}O_3$ (BTS) system. We have kept processing parameters exactly same as were for the synthesis of composites discussed in the last chapter.

6.2 Results and Discussion

In the present chapter, a synthesis of (x) $BaTi_{0.85}Sn_{0.15}O_3$ (BTS) – (1-x) CNT (x = 5, 10, 15, 20 wt. %) composites was carried out using mechanical milling of the BTS powder prepared by solid state reaction method. The multiwalled CNT used in this work was synthesized by one step spray pyrolysis techniques using benzene ferrocene precursors.

6.2.1 Thermal Analysis

Thermal analysis (TG and DSC) of the synthesized CNT and mixture of powder obtained after milling for one of the composite BTS-CNT20 was carried out using simultaneous TG-DSC (Mettler Toledo) thermal analyzer in the temperature range 30–1000 °C with a heating rate of 10 °C/min in nitrogen atmosphere. TG and DSC analysis were employed to examine the thermal stability of the as prepared carbon nanotubes and carbon nanotubes after mixing with BTS powder in ball mill for 4 hrs. TG-DSC curves of the CNT and mixture for one of the composite BTS-CNT20 are shown in Figure 6.2 and 6.3 respectively. The TG curve of CNTs shows weight remains almost constant up to 600^{o}C. The weight starts decreasing linearly up to the highest temperature of the measurement i.e. 1000 ^{o}C. In the temperature range 600-1000^{o}C

weight loss is found to be approximately 56.48%. In the entire temperature range of measurement no peak in DSC curve due to exothermic or endothermic reactions was observed. Figure 6.3 display TG and DSC curve of the mixture of BTS and 20 % CNT. TG curve of mixture of composite shows weight loss approximately 20.03 % in the scanning temperature range from 27 to 1000 ^{o}C. Total weight loss is occurring in two steps. The first step weight loss (2.87%) recorded in the temperature range 27- 104 ^{o}C may be related to the loss of volatile species, absorbed water molecules and remaining acetone used in the mixing. The second step weight loss approximately 17.16 % between 500- 600 ^{o}C is attributed to the decomposition of carbon nanotubes present in the mixture. It is worthwhile to mention that observed weight loss 20.03 % is same as of the weight % of the CNT used in the synthesis of the composite BTS-CNT20. In the DSC curve of the mixture a broad exothermic peak approximately at 600^{o}C was observed which is attributed to the burn of formed carbonaceous material CNT [214]. Similar results were obtained from the thermal analysis of the mixture of BTS and CNT for other composites.

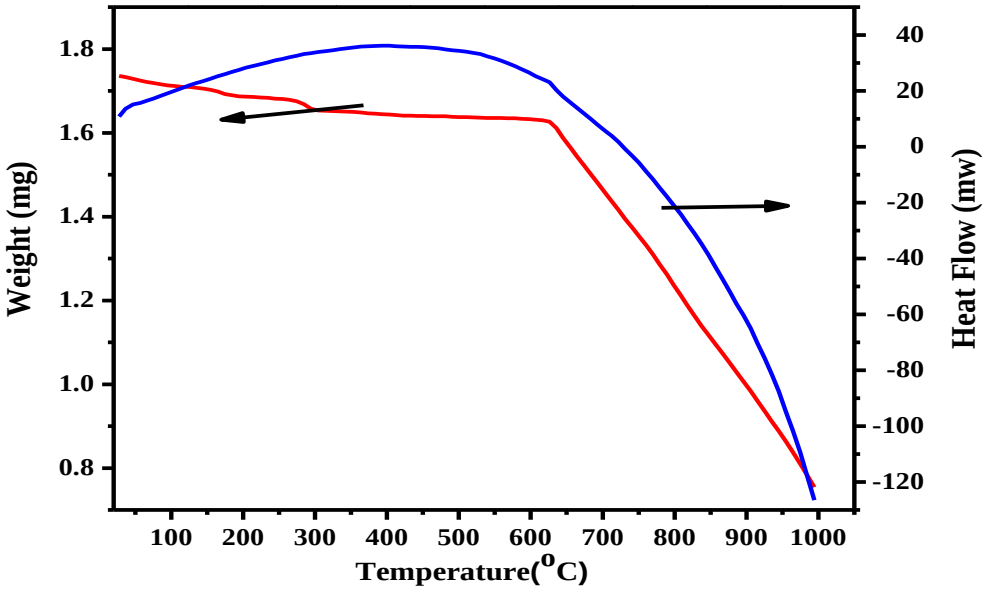

Figure 6.2 TGA-DSC curve of precursor CNT

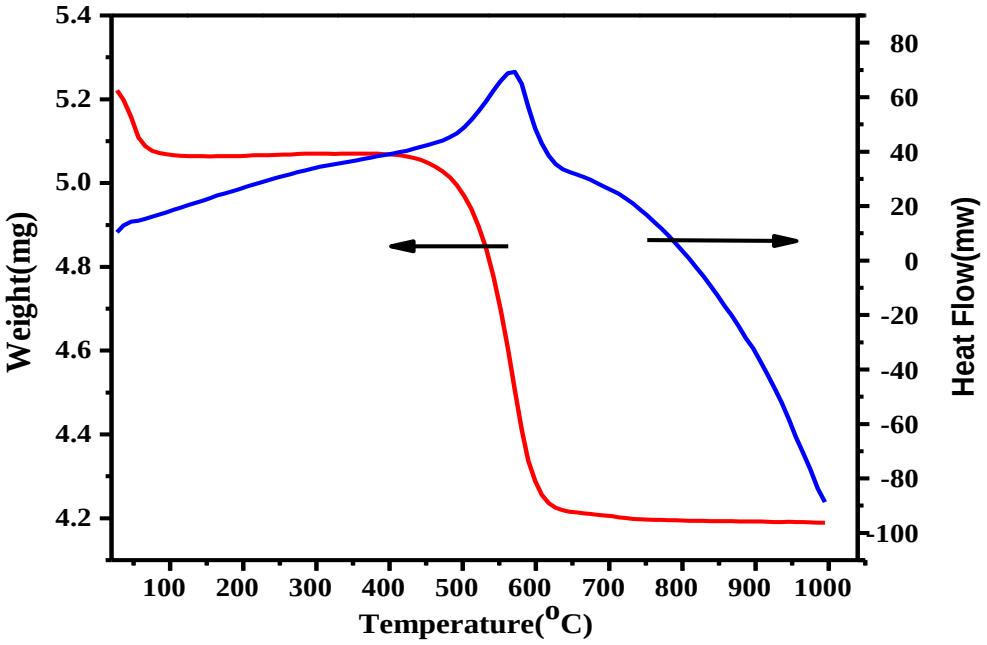

Figure 6.3 TGA-DSC curve of mixture of composite BTS15-CNT20

6.2.2 Phase Analysis

In order to do the analysis of phase formation, the room temperature powder XRD patterns of constituent phases BTS and CNTs and their composites of BTS-CNT5, BTS-CNT10, BTS-CNT15 and BTS-CNT20 have been recorded and shown in Figure 6.4. The observed peaks in the XRD patterns of BTS are duly assigned with the help of JCPDS file (No. 31-0174) reported in the literature for cubic phase of $BaTiO_3$. XRD pattern of CNT showed a broad peak at 22.1 ^{o} corresponding to (002) plane of typical multi-walled CNTs [215,216]. The XRD pattern of the composites was matched with XRD patterns of constituent BTS and CNT. All the observed peaks present in the XRD pattern of the composites are matched well with constituent BTS, no peaks corresponding to CNT was observed. There is also no additional peaks corresponding to impurity, secondary phases are present in the diffraction pattern, suggests that during formation of composite no new phase has been formed due to possible reactions between the components. The suppression of CNT peak in the composites may be due to high crystallinity of BTS as compared to CNT. In order to gain more information from the XRD data enlarge view of highest intensity peak corresponding (101) plane of BTS is obtained and shown in Figure 6.4. From the Figure 6.4 it is infer that as concentration of CNT increases in the composite peak gets broader and broader which indicates decrease in the crystallite size. It seems that presence of CNTs in the powder of BTS is acting as grain growth inhibitors. The decrease in the crystallite size may possible due to presence of CNT in between the grains of the BTS during sintering process. Further it is noticed that there is no appreciable shift in the position of the peak which ruled out diffusion or substitution of any element from the CNT into BTS lattice. The average crystallite size (D) of the BTS, CNT and synthesized composites was calculated from the X-ray line broadening of (101) and (002) peak using Scherer's formula given by Equation (2.2). The width of the Bragg peak observed in XRD is the combination of various

factors like instrumental broadening, lattice strain and size of the sample, etc. In order to separate out these contributions, it is necessary to collect the additional diffraction pattern from line broadening of the standard model such as silicon to determine the instrumental broadening. Now the β corresponding to the most intense peak is estimated using the relation;

$$\beta^2 = (\beta^2)_{measured} - (\beta^2)_{instrumental} \quad (6.1)$$

After subtracting of the instrumental broadening using Equation 6.1, the crystallite size for all samples has been calculated using Equation (2.2) and listed in Table 6.1.

Table 6.1 Phase fraction ratio, crystallite size and grain size of sintered samples

Sample code	**Phase Fraction Ratio**		**Crystallite size(nm)**	**Grain Size(μm)**	**Experimental Density(g/cc)**	**Theoretical density(g/cc)**	**Porosity (%)**
	BTS	**CNT**					
BTS	1.00		45.2	4.50	6.01	6.02	0.16
BTS-CNT5	0.95	0.05	30.1	3.00	5.70	5.83	2.22
BTS-CNT10	0.90	0.10	29.0	1.50	5.42	5.66	4.60
BTS-CNT15	0.85	0.15	26.3	0.74	5.24	5.49	4.55
BTS-CNT20	0.80	0.20	24.7	0. 52	5.02	5.32	5.63
CNT	--	1.00	5.3	Length=842 nm Diameter=82 nm	--	2.60	--

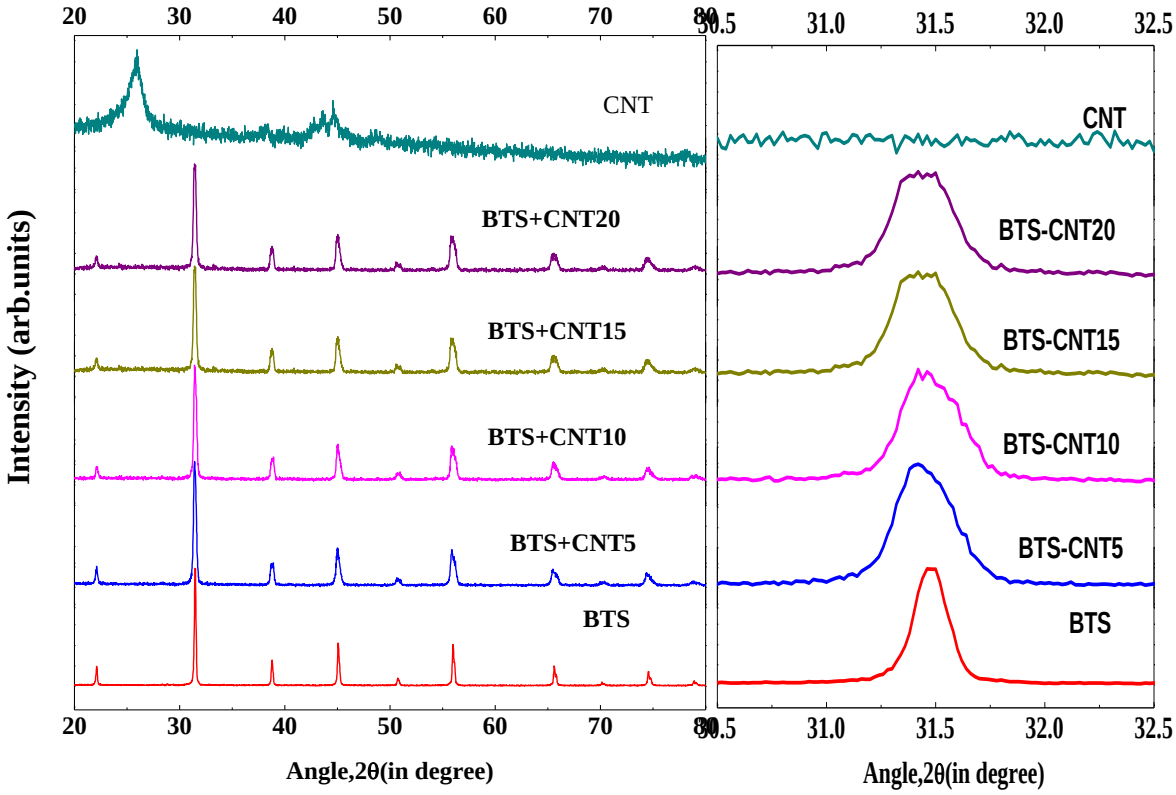

Figure 6.4 The x-ray diffraction pattern of composites and their end members

6.2.3 Fourier Transform Infrared (FTIR) Spectroscopy

Fourier transform infrared (FTIR) spectroscopy was carried out in the range of 400–4000 cm^{-1}. The FTIR spectrum of BTS, CNT and one of the composite BTS-CNT20 are shown in Figure 6.5. The FTIR spectrum of BTS was compared with the FTIR spectra of barium titanate and Barium stannate. From the literature, it is noted down that in the FTIR spectrum of barium titanate shows a strong peak around 550 cm^{-1} assigned to Ti-O stretching vibrations [217,218]. Therefore, the observed broad peak in the FTIR spectrum of sample BTS is also assigned to Broadness in the peak of BTS as compared to $BaTiO_3$ may be due to existence of Sn-O

vibrations. FTIR spectrum of the composites is similar to that of BTS. Intensity and position of Ti/Sn-O stretching vibrations in the FTIR spectrum of the composites remained unchanged indicating that the MWCNTs have not been able to modify the intrinsic structure of barium titanate. On careful observation of the FTIR spectrum of the composites it is found that spectrum also contains two weak peaks at 1205 and 1580 cm^{-1} shows, which could be assigned to carbon skelton and presence of the cylinder like carbon structure of MWCNTs [219,220].

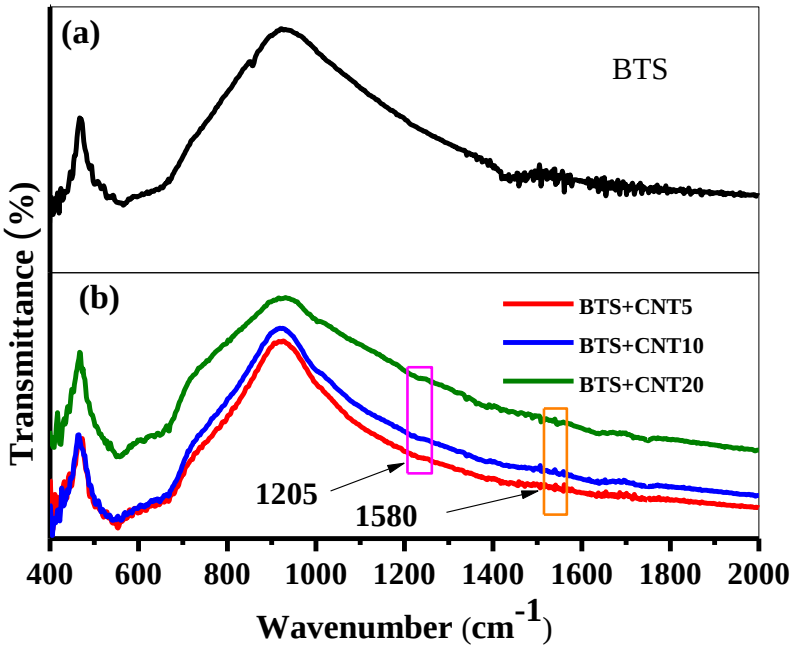

Figure 6.5 Fourier transform infrared (FTIR) spectra of (a) BTS (b) composites of BTS-CNT

6.2.4 Surface Morphology Analysis

Scanning electron micrographs (SEM) of the fractured surfaces were obtained to get information about grain size, shape and the degree of interaction between two phases BTS and CNTs. The SEM images of the fractured surfaces of BTS and composites BTS-CNT5, BTS-CNT10, BTS-CNT15 and BTS-CNT20 were recorded at different magnifications. SEM images

at three different magnifications are shown in Figure 6.6. Due to lower dimensions of CNTs, field emission scanning electron micrographs (FE-SEM) of the synthesized multiwalled CNTs were recorded and in the same figure. The average grain size of samples was determined by the Gaussian distribution function method using software 'Image J' and is given in Table 6.1. From the Table 6.1 it is noticed that average grain size of BTS powder used in the composites is 4.5 μm. Morphology of the grains of BTS is spherical and distribution in the grain size is narrow. Microstructure of the composites exhibited two types of morphology of the grains; spherical and rod like. At low magnification it is noticed that rod like structure is uniformly distributed in the matrix spherical shaped grains rather than aggregating at the grain boundaries. We have assigned spherical shaped grains to BTS and rod like structure to the CNTs. Further, it is observed that increasing CNT content in the composite has resulted in the formation of smaller BTS grains than those formed in pure BTS. The average grain size of pure BTS is 4.5 um while it is found to be 0.52 um for the composite BTS-CNT20. It has been reported in the literature that the presence of CNT in ceramic matrices acts as 'grain refining agent' by effectively suppressing material transport through GB regions during sintering and hence reduction in the size of the grains [221,222]. The inhibition of ceramic matrix grain growth through adding carbon nanotubes is very common phenomenon. No hole surrounding the CNTs is observed even on the fractured surfaces which indicate that tight binding between the BTS and CNTs has been achieved. There is no obvious border between the rod like CNTs and the BTS matrix (Fig. 6.6), which will ensure the perfect coupling of mutual mechanical, electrical and thermal properties. Composites are sintered densely and have few pores between grains.

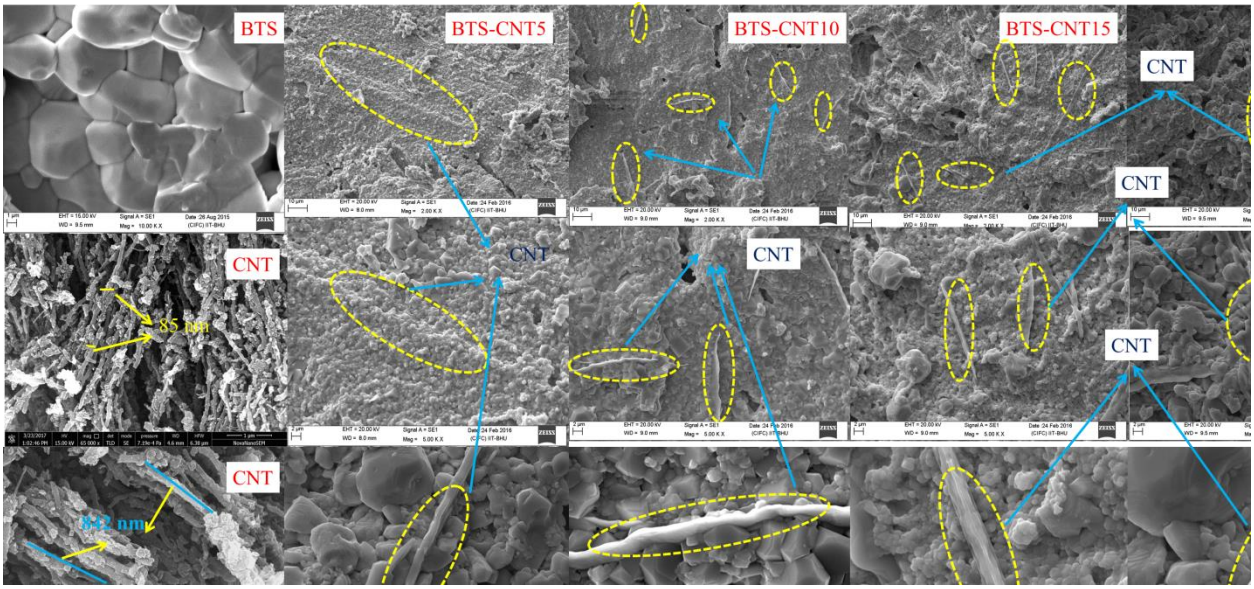

Figure 6.6 Scanning electron micrographs (SEM) of the fractured surfaces at different magnifications

In order to gain more understanding about the microstructure of composites, micrographs were recorded at the highest magnification i.e at 20,000 of the used scanning electron microscope. From the high magnification images it is clear that thickness of the rod like structure present in the microstructure of the composites lies between 0.5-2.0 µm. The average length and diameter of synthesized CNTs were obtained from FE-SEM images using software 'Image J' is 842 nm and 82 nm, respectively (given in Table 6.1). Large thickness of the rods present in the composites may be due to coating of BTS particles on the surface of the CNTs. Moreover, thickness of the rod is not uniform which also supports existence of BTS particles on the surface of CNTS. In order to confirm coating of BTS at the surface of the CNTs elemental analysis using energy dispersive x-ray analysis (EDXA) technique has been used and discussed below.

6.2.5 Energy-Dispersive X-ray (EDX) Analysis

To check the compositional homogeneity of the synthesized samples, the compositional variation (regarding concentration profile of the elements) has been probed by recording EDXA spectra of different points randomly selected in various spherical grain cores and grain boundaries. Typical EDXA spectra of the samples are shown in Figure 6.7. It is noted that only peaks of Ba, Ti, Sn and O are present in the EDXA spectra of the samples. All the constituent elements observed in the spectrum of the samples are as per their expected concentrations. In order to confirm deposition of BTS grains on the surface of the CNTs we have recorded concentration prolife of the elements present at marked positions on the surface of the rods. The concentration profile along with microstructure for two composites BTS-CNT10 and BTS-CNT20 are shown in Figure 6.8. From the concentration prolife it is found that Ba, Ti, Sn, O, C and Fe elements are present. Presence of Ba, Sn and Ti elements on the surface of the rod confirms coating or deposition of BTS particle on the surface of CNTs. We have carried out elemental analysis of the synthesized CNTs which is shown in Figure 6.6. EDX spectrum of the CNTs exhibited presence of elements C and Fe. The present Fe element in the CNTs and the composites may be due to use of the ferrocene in the synthesis of CNTs.

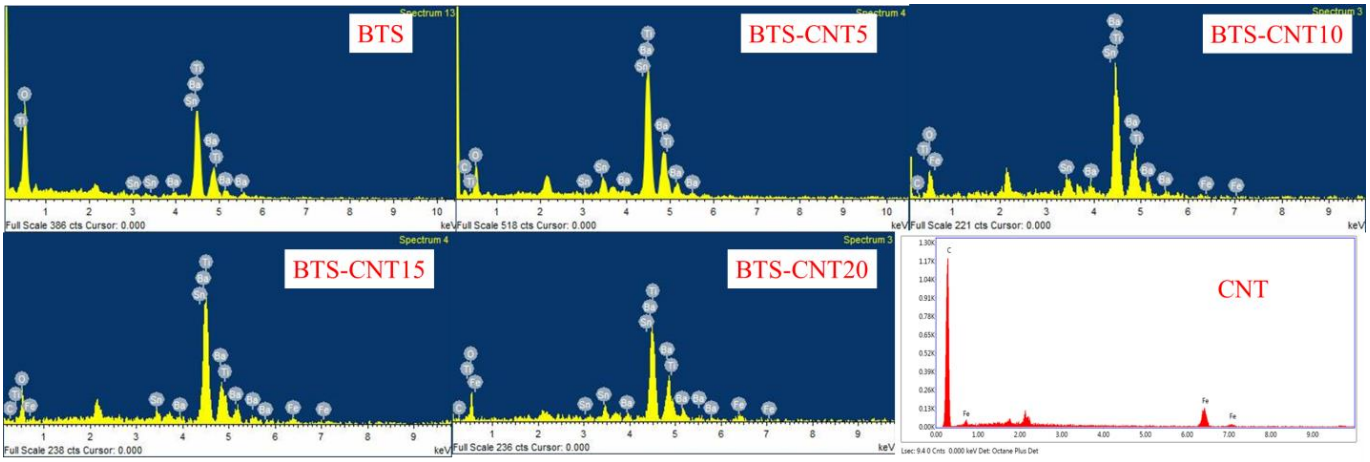

Figure 6.7 Energy dispersive x-ray analysis (EDXA) of pure BTS and composites of BTS-CNT

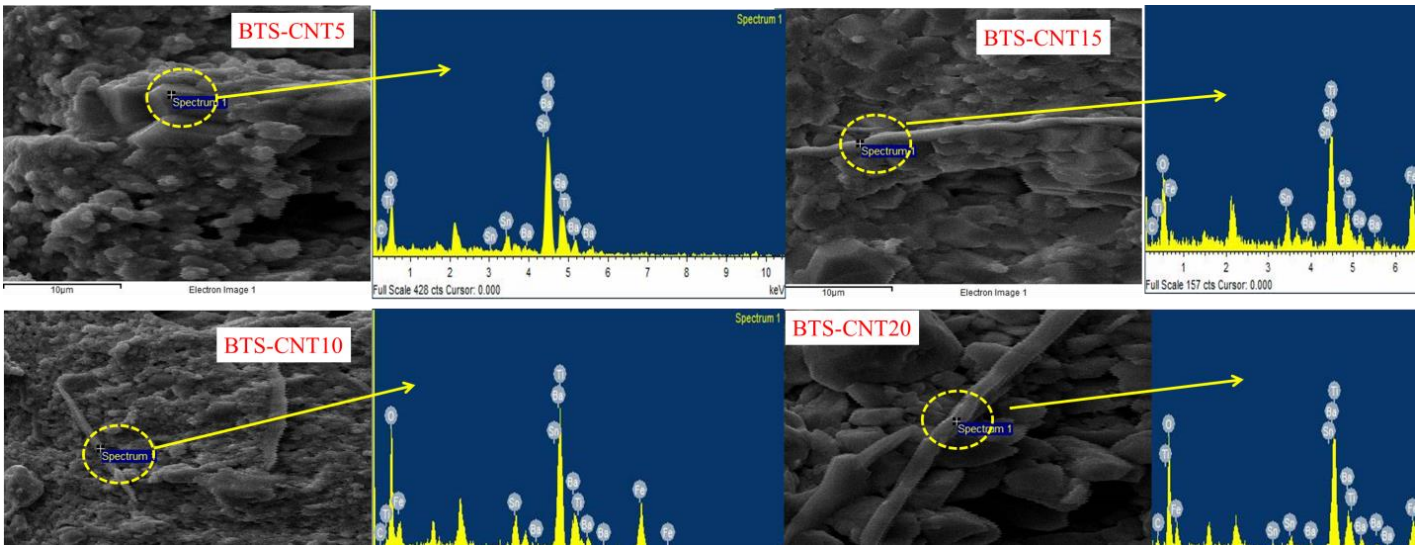

Figure 6.8 Energy dispersive x-ray analysis (EDXA) of pure BTS and composites of BTS-CNT at focused view of CNT

6.2.6 Dielectric Analysis

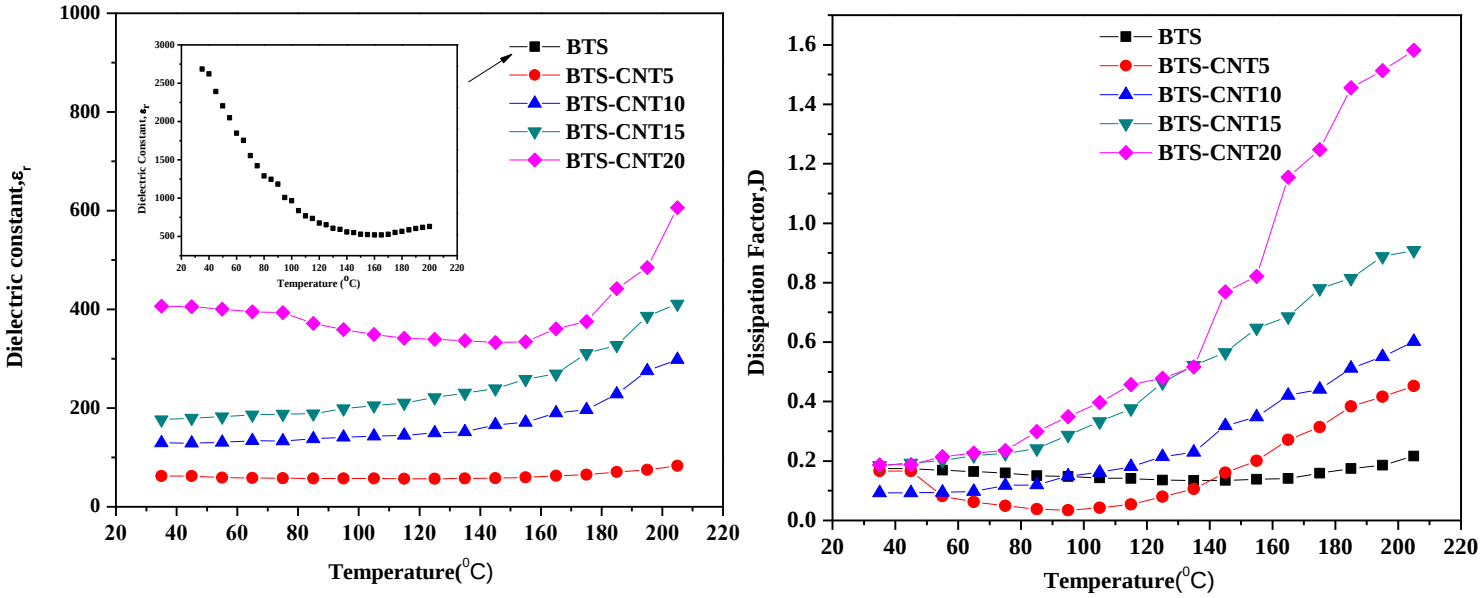

Figure 6.9 Variation of Dielectric constant, Dissipation factor with temperature for BTS-CNT Composites

The variation of the dielectric constant (ε_r) and dissipation factor (D) with temperature of the samples at 1 kHz frequency is shown in Figure 6.9. Due to higher value of dielectric constant of BTS (approximately one order) as compared to the composites variation is shown in the inset of the Figure 6.9. Figure 6.9 shows that the dielectric constant of BTS decreases almost linearly with increasing temperature. Variation of the dielectric constant of composites remains almost constant up to 150^{o}C thereafter start increasing with increasing temperature. As it is already mentioned in the hopping of electrons/ions from one lattice site to another lattice site is a thermally activated process therefore increasing temperature may lead to the increase in dielectric constant. Dielectric constant (at room temperature and 1 kHz) of BTS, BTS-CNT5, BTS-CNT10, BTS-CNT15 and BTS-CNT20 is presented in Table 6.2. From the Table 6.2 it is noticed that value of dielectric constant of the composites is lower than the dielectric constant of

BTS. The lower value of dielectric constant of the composites may be due to the higher lower value of the conductivity as compared to BTS because conductivity of multiwalled CNTs is high (~ 10^4 ohm-cm^{-1}) [223]. The variation of dissipation factor, D with temperature is similar for BTS and composites. Dissipation factor remains constant up to 100^{o}C and thereafter starts increasing with increasing temperature. Value of dissipation factor of all the samples at room temperature is presented in Table 6.2 one can notice that value of dissipation factor (at RT and 1 kHz) of the composites is slightly higher than that for BTS which is may be attributed to higher conductivity of the composites. The difference in the value of dissipation of BTS and composites increases with increasing temperature.

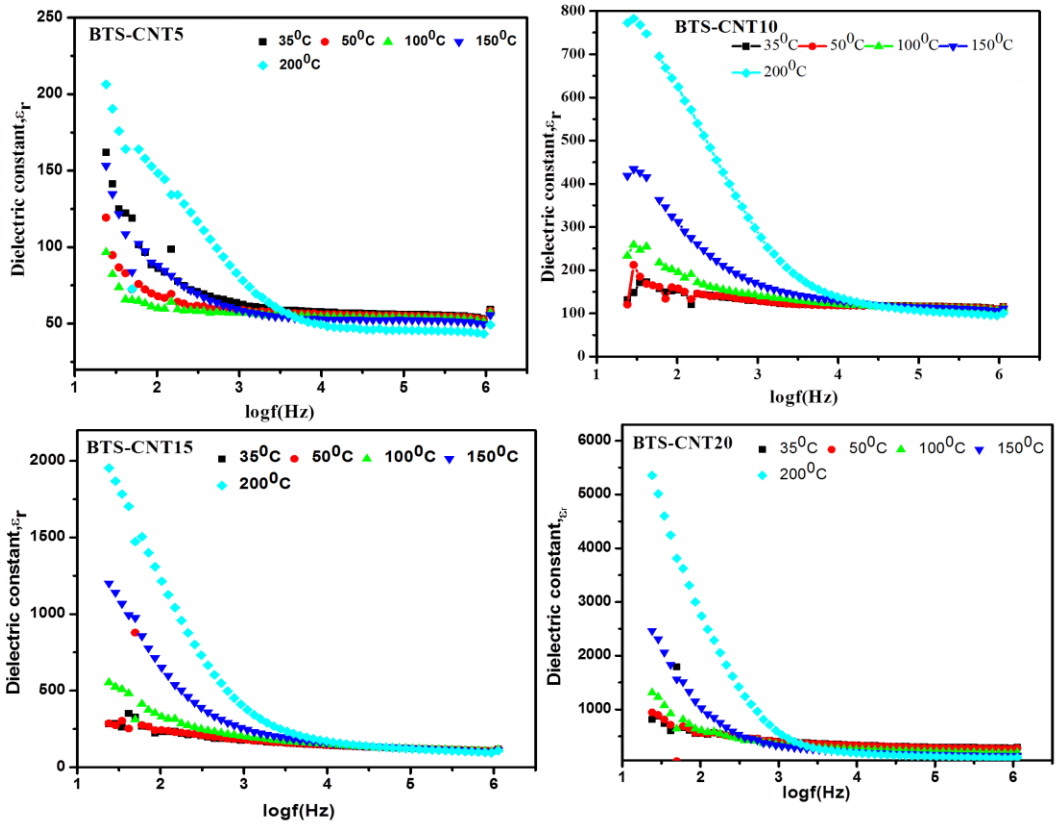

Figure 6.10 The variation of dielectric constant as function of frequency at different temperature

Figure 6.10 and 6.11 shows a variation of dielectric constant and dissipation factor with frequency at few selected temperatures composites. The dielectric constant of BTS as well as of composites decreases with an increase in the frequency upto 10 kHz and becomes constant above this frequency. The large values of dielectric constant in the low-frequency region of the samples can be assigned to the space charge polarization and inhomogeneous dielectric structure. These inhomogeneities arise from impurities, grain structure and pores etc. [223]. The space charge polarization dominates at low frequency and high temperature. The decrease in dielectric constant with frequency can be explained by Koop's theory [224], which considers the dielectric of ceramic bodies as the Maxwell–Wagner type inhomogeneous medium of two layers [225,226]. According to this model, the dielectric structure contains conducting grains which are separated by insulating grain boundaries. At lower frequencies, the effect of grain boundaries dominates over grains. If the resistance of the grain boundary is high, the electrons reach the grain boundaries through hopping, pile up and hence, in turn, produce polarization which accounts for the high value of dielectric constant [227,228]. However, as the frequency increases, the decrease in dielectric constant is observed because, at high frequencies, the electrons at the grain boundaries generally reverse their direction of motion. This reduces the probability of electrons reaching the grain boundary and hence results in the reduction in the dielectric constant. In composites presence of CNTs at grain boundaries will reduce polarization at grain and grain boundaries of BTS and weaken diminish which may be the reason for the lower value of the dielectric constant.

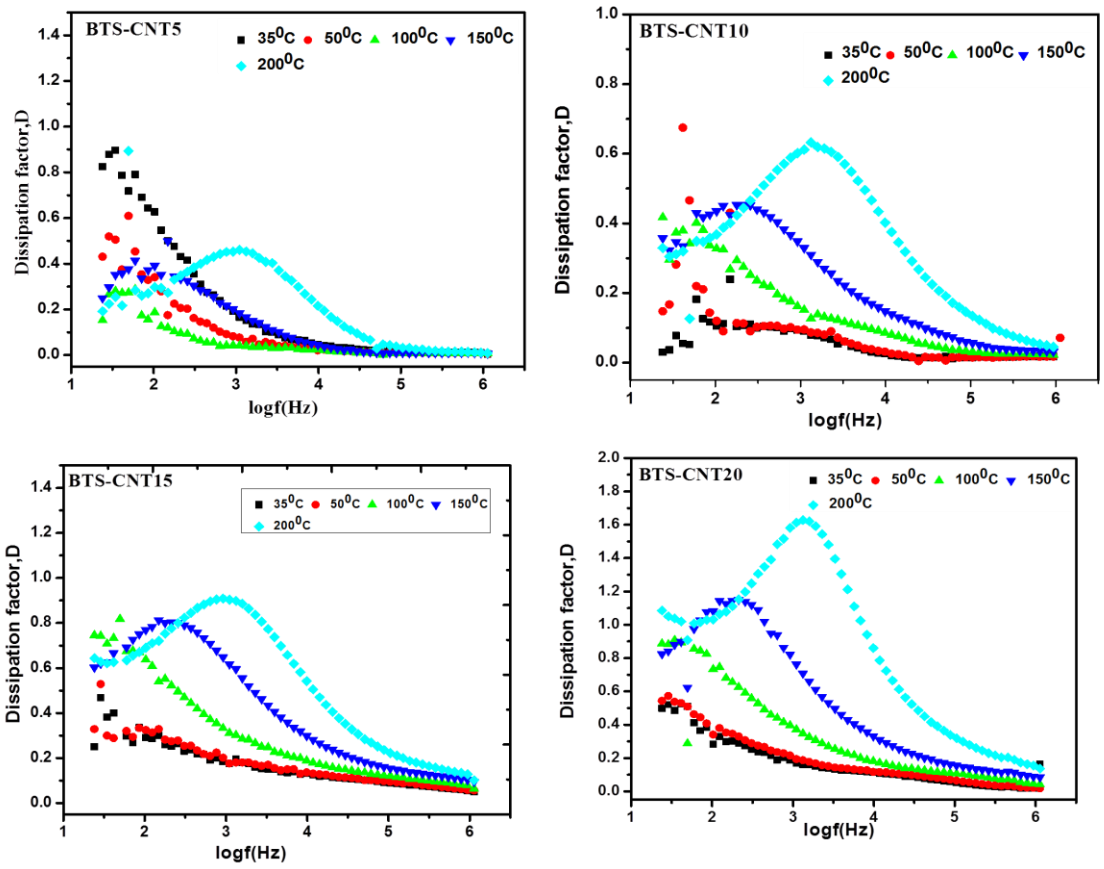

Figure 6.11 The variation of dissipation factor as function of frequency at different temperature

Variation of dissipation factor, D with log f for BTS and composites are shown in Figure 6.11, a peak is observed at temperatures above 100^{o}C which shifts towards higher frequency side as temperature increases. This results suggests that a thermally active process of polarization is operative in all the samples. The presence of peak in D vs. log f plots may also be due to the relaxor nature of the BTS as it is mentioned in the previous chapters.

6.2.7 AC Conductivity

AC conductivity (σ_{ac}) of BTS and composites has been measured in the frequency range 40Hz - 2 MHz and temperature range 30- 200^{o}C to understand conduction

mechanism involved in these samples. Figure 6.12 shows a plot of AC conductivity (σ_{ac}) versus weight % of CNTs in the composite of BTS-CNT at room temperature and 1 kHz frequency.

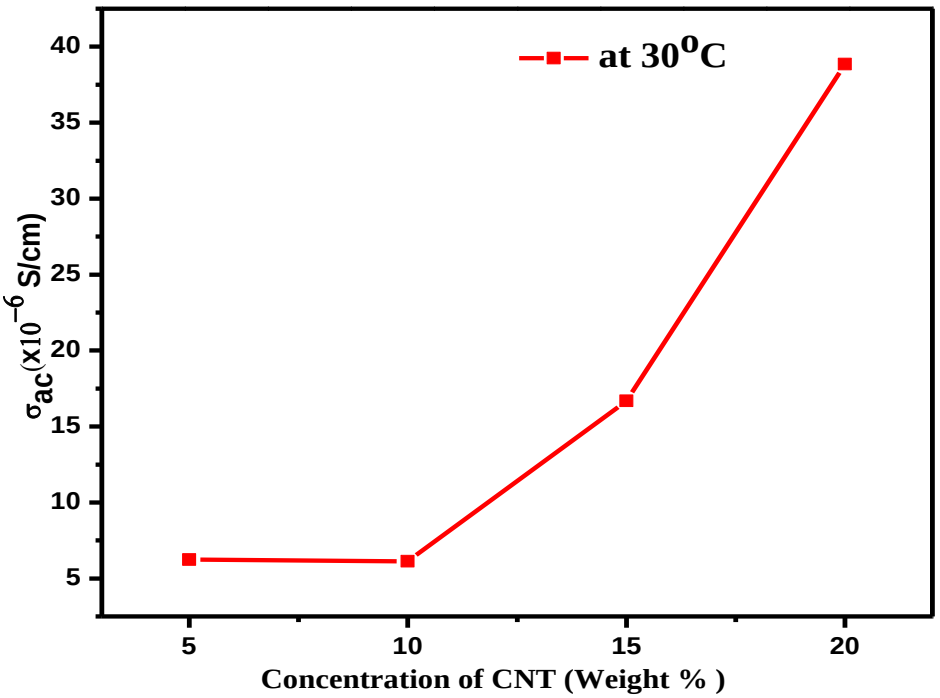

Figure 6.12 Variation of conductivity with weight % of CNT at1kHz frequency.

Value of σ_{ac} of the samples at room temperature and 1 kHz frequency is listed in Table 6.2. It is noticed from the table that the electrical conductivity of BTS at RT is $5x10^{-6}$ S/cm whereas of the composite with highest amount of CNT i.e. BTS-CNT20 is 40x 10^{-6} S/cm on addition of CNT. This result is contradictory to the results obtained by other researchers that on addition of small amount of CNTs in the ceramic matrix conductivity increases by many orders of magnitude [229]. We believe that large enhancement in the conductivity is only possible when CNTs are interconnected in the matrix of the BTS. From the SEM image of the composites (as discussed

above) is obvious that CNTs are not interconnected inside matrix of ceramic BTS [230]. Absence of continuous conducting paths may be the reason for low value of the conductivity of the composites instead of our expected to get high value of the conductivity of the composites.

Table 6.2 Room temperature physical parameter (Dielectric constant, Dissipation factor and ac conductivity) for composites

Composite	Physical parameter at room temperature		
	ε_r (Dielectric constant)	Dissipation factor, D	σ_{ac} (1 KHz)
BTS	2684.42	0.17513	3.38×10^{-6}
BTS-CNT5	62.20	0.16586	4.70×10^{-6}
BTS-CNT10	129.26	0.09259	8.68×10^{-6}
BTS-CNT15	176.67	0.1846	17.32×10^{-6}
BTS-CNT20	406.48	0.18694	40×10^{-6}
CNT	--	--	--

Variation of $\log_{10}\sigma_{ac}$ with $\log_{10}$ f of all BTS (as discussed in chapter 3) and composites at few selected temperatures are shown in Figure 6.13. From this figure it is noticed that nature of variation of conductivity with frequency of all the samples are more or less the same. Variation of conductivity with frequency is almost linear in the entire range of frequency measurement. Effect of temperature on the conductivity is almost negligible.

In general the total conductivity is combination of two contributions; one is dc conductivity (σ_{dc}), frequency independent part of the plot which is low frequency plateau. The second part is ac conductivity, σ_{ac} (frequency dependent part of the spectrum) which increases

with frequency. Johnscher's proposed an equation to describe the frequency dependence of total conductivity σ_{total} (f) as follows [231];

$$\sigma_{total}(f) = \sigma_{dc} + A\omega^{n} = \sigma_{dc}[1+(f/f_H)^{n}] \quad (6.2)$$

Where f_H is the hopping frequency (frequency at which crossover from dc to the dispersive conductivity takes place), A is a parameter which is temperature activated and power exponent **n** , represents the electrical relaxation behavior of the material whose value lies between 0 to 1.

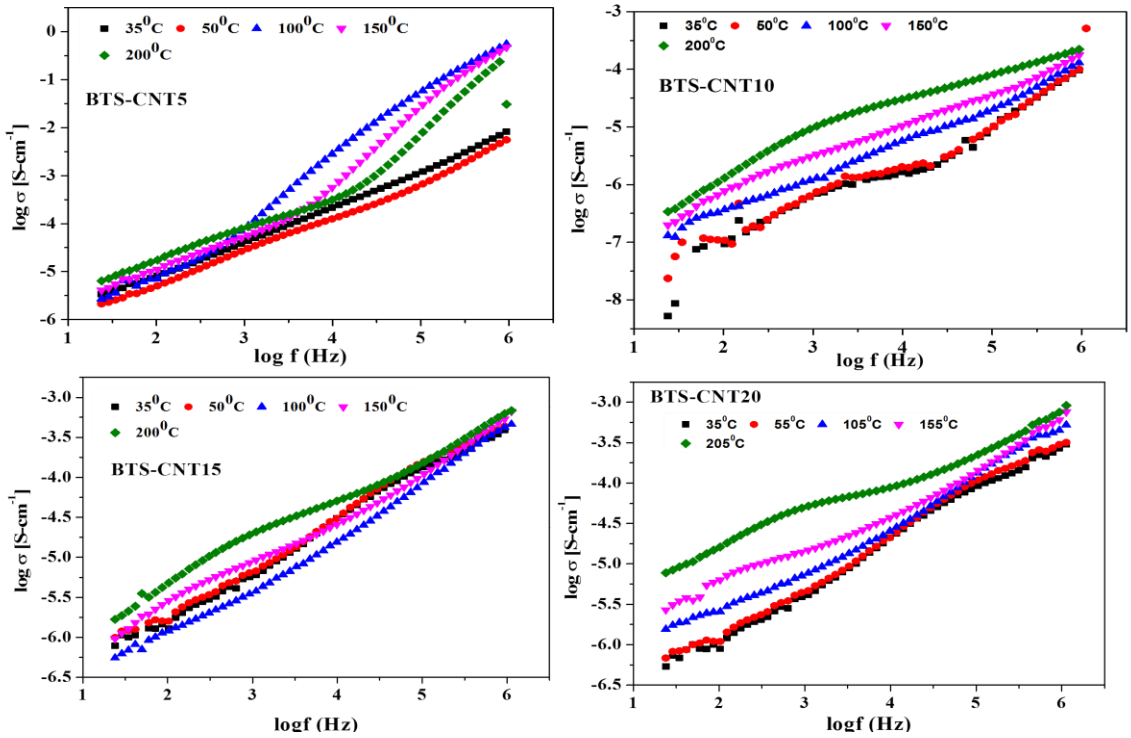

Figure 6.13 Variation of logarithmic of ac conductivity with logarithmic of frequency for composites BTS-CNT at different temperatures.

In Figure 6.13 the room temperature conductivity does not show frequency independent part of conductivity due to limited range of frequency measurement. Frequency independent part may be present below 40 Hz frequency. The variation of room temperature conductivity at 1Khz frequency shows with incorporation of CNT in the composite the conductivity increases due to

presence of small amount of Fe in the composite. The presence of Fe also confirm from their EDX spectrum analysis.

6.3 CONCLUSION

Composites of BTS and multiwalled CNTs have been synthesized successfully by solid state reaction method. . Thermal gravimetric analysis (TGA) of mixture of BTS and CNTs indicated that thermal decomposition temperature of CNTs has reduced after mixing. In the XRD pattern of the composites, peak corresponding to CNT are absence which is attributed to lower crystalinity of CNTs as compared to BTS. FTIR spectrum of the CNTs confirmed presence of carbon Skelton in the composites. Scanning electron micrographs (SEM) images displayed rod like structure of CNTs in the microstructure of the composites. EDXA analysis confirmed the presence of BTS particles on the surface of CNTs. Dielectric constant of the composites is lower than that of BTS. Dissipation factor of the composites is more than that of BTS. AC conductivity of composite BTS-CNT20 is 8 times higher than that of the conductivity of BTS. The AC electrical conductivity is found to vary linearly with frequency in these composites within the frequency range of measurement (40 Hz- 2MHz).